

The Oxidation Behavior of a Si-Ti-C-O Fiber with a Low Oxygen Content

Ken-ichi KAKIMOTO, Toshio SHIMOO* and Kiyohito OKAMURA*

Graduate Student, University of Osaka Prefecture, 1-1, Gakuen-cho, Sakai-shi 593

*Department of Metallurgy and Materials Science, College of Engineering, University of Osaka Prefecture, 1-1, Gakuen-cho, Sakai-shi 593

低酸素 Si-Ti-C-O 系繊維の酸化挙動

柿本健一・下尾聡夫*・岡村清人*

大阪府立大学大学院生, 593 堺市学園町 1-1

*大阪府立大学工学部材料工学科, 593 堺市学園町 1-1

[Received November 4, 1994; Accepted March 14, 1995]

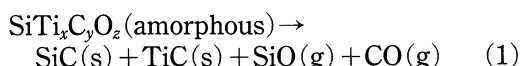
The oxidation behavior of a Si-Ti-C-O fiber with a low oxygen content of 6 mass% has been investigated. The kinetic data of the fiber were expressed by the contracting-cylinder formula. The activation energies were calculated to be 72 and 430 kJ/mol at the low-temperature ($T < 1473$ K) and the high-temperature ($T > 1473$ K) regions, respectively. An oxide film consisted of SiO_2 and TiO_2 ; and the former was amorphous during the low-temperature oxidation process tending to be crystallized into cristobalite at higher temperatures. When the fiber was oxidized at 1773 K, the interface between the oxide film and the unoxidized core fiber contained many microcracks; moreover, the core fiber lost 75% of its original strength at room temperature.

Key-words: Silicon-titanium-carbon-oxygen amorphous fiber (Tyranno fiber), Oxide layer, Cristobalite, Activation energy of oxidation, Tensile strength of fiber

1. Introduction

Since the development of silicon carbide (SiC) fiber,¹⁾ which can be obtained by melt-spinning and thermal decomposition of polycarbosilane (PC), the polymer precursor method has been widely utilized to prepare silicon carbide-like or silicon nitride-like ceramic fibers. Advantages of ceramic fibers from precursors are the ability to control crystallite size and to prepare continuous fine-diameter fibers which are suitable for weaving and knitting.²⁾

Following the SiC fiber, polytitanocarbosilane (PTC)-derived amorphous Si-Ti-C-O fiber (Tyranno; Ube Industries Co., Ltd., Japan) has been manufactured using the thermal oxidation curing process which cross-links the polymer by oxygen to make the fiber infusible.³⁾ This fiber has high tensile strength and modulus; there is an increasing interest in the use of the fiber as reinforcement of metal-, glass- and ceramic-matrix composites.⁴⁾ This fiber, however, pyrolyzes by exposure at high temperatures above 1500 K in Ar stream, where evolution of SiO and CO gases occurs by the following Reaction (1):⁵⁾



And then, SiC and TiC crystallized. The morphology and crystal structure of the fiber change and the tensile strength rapidly decreases; therefore, it is necessary to control the oxygen content, which is responsible for the gas evolution, in order to improve the tensile strength at higher temperatures. Okamura et al.⁶⁾ reported an oxygen-control curing process using radiation-chemical reactions. Si-Ti-C-O fiber with a low oxygen content (6 mass% oxygen) has been very recently prepared by electron beam curing, and had lower pyrolytic rate than the commercial fibers (18 and 13 mass% oxygen) at high-temperatures.⁷⁾

On the other hand, oxidation of the fiber occurs at high-temperatures in oxidizing atmospheres. We have found in commercial Si-Ti-C-O fibers that (1) the oxidation rate of the fibers was controlled by diffusion process across a protective oxide film, consists of SiO_2 and TiO_2 , formed on the fiber surface,⁸⁾ and (2) the pyrolysis of the fibers was suppressed appreciably by presence of the surface oxide film.⁹⁾ In this paper, we report the oxidation behavior of Si-Ti-C-O fiber with a low oxygen content and compare it with that of the commercial fibers for the purpose of pointing out the influence of the oxygen content.

2. Experimental procedure

2.1 Sample preparation

The fiber specimen used in this study was experimental Si-Ti-C-O fiber produced by Ube Industries Co., Ltd., Japan. This fiber had been cured using an electron beam accelerator at Takasaki Radiation Chemistry Research Establishment, Japan Atomic Energy Research Institute (JAERI). Irradiation curing was attained in He stream with an overall irradiation dose of 15 MGy. The cured fiber was subjected to heating treatments, which corresponds to the organic-inorganic transition, at 1573 K in N_2 stream following a preheating at 650 K in Ar stream. Its chemical composition corresponds to the overall formula $\text{SiTi}_{0.02}\text{C}_{1.57}\text{O}_{0.21}$ (with trace amounts of hydrogen), i.e., the oxygen content of the fiber is 6 mass%. Table 1 shows various properties of the Si-Ti-C-O fibers having different content of oxygen (a

Table 1. Various Properties of Si-Ti-C-O Fibers with Various Oxygen Contents

Sample code (mass%Oxygen)	Heating temperature (T/K)	Composition	Curing method	Diameter ($d/10^{-6}\text{m}$)	Density ($\rho/\text{Mg}\cdot\text{m}^{-3}$)
STC(6)	1573	$\text{SiTi}_{0.02}\text{C}_{1.57}\text{O}_{0.21}$	Electron beam	10.0	2.39
STC(13)	1573	$\text{SiTi}_{0.02}\text{C}_{1.33}\text{O}_{0.44}$	Thermal oxidation	8.5	2.38
STC(18)	1573	$\text{SiTi}_{0.02}\text{C}_{1.40}\text{O}_{0.64}$	Thermal oxidation	8.5	2.33

new and two commercial fibers). These three fibers were named STC(6), STC(13) and STC(18), respectively, on the basis of its oxygen content.

The fiber was cut into lengths of 30 mm and then heat-treated in Ar stream at 1073 K for 1 h to remove sizing agents. Crystalline of the desized fiber was proved to unchange from that of the sized one, using transmission electron microscope (TEM) and X-ray diffraction (XRD).

2.2 Characterization

The oxidation mechanism of Si-Ti-C-O fiber was studied by thermogravimetric (TG) analysis. An experimental temperature, which was measured by a PtRh 40%-PtRh 20% thermocouple, was kept constant at 1273, 1373, 1473, 1573, 1673, and 1773 K. We suspended the MgO crucible, in which the fiber was placed, in the hot zone of a SiC resistance furnace equipped with a thermobalance unit. O_2 gas was introduced from the bottom of an Al_2O_3 reaction tube and exhausted from the top of it. The gas flow rate was fixed at $2.5 \times 10^{-5} \text{ m}^3/\text{s}$. The mass change of the fiber was measured continuously. After the oxidation test for 64.8 ks, the fiber was cooled rapidly at a rate of 500 K/s to room temperature. Fiber samples were ground into powders and XRD patterns were obtained to examine the reaction products. The surface and the fractured surface of the fibers were observed by scanning electron microscope (SEM). Samples for TEM (JEM-2000FX, 200kV, JEOL) analysis were prepared by mounting ground samples on a thin copper mesh which was previously coated with a thin layer of carbon. The tensile tests of the fiber after the removal of an oxide film with $\text{NH}_4\text{F} + \text{HF}$ solution were made at room temperature by a monofilament method using a universal testing machine (Tensilon UTM-II-20; Toyo Measuring Instrument Co., Ltd., Japan), where a load cell, gauge length and crosshead speed were 100g, 10 mm and 2 mm/min, respectively. Twenty fibers were tested to determine the average tensile strength. The diameter of each core fiber was measured three times using an optical microscope equipped with a filar eyepiece.

3. Results and discussion

3.1 The oxidation kinetics of the fiber

Figure 1 shows the effects of oxidation time on the

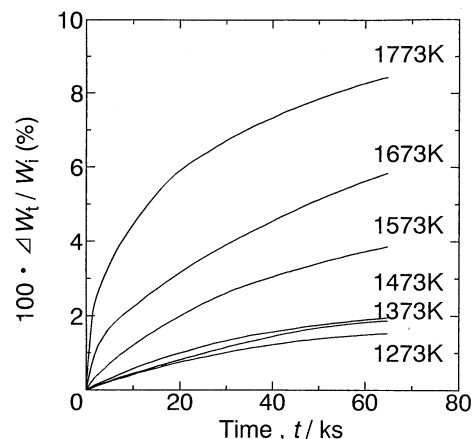
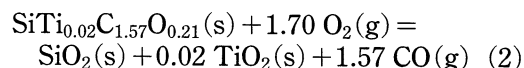


Fig. 1. Relationship between $\Delta W_t/W_t$ ratio and oxidation time for STC(6), where ΔW_t stands for mass gain and W_t is the initial fiber mass.

$\Delta W_t/W_t$ ratio of STC(6) for various heat treatment temperatures, where ΔW_t stands for mass gain measured by the thermobalance, and W_t is the initial fiber mass. The oxidation reaction of STC(6) is expressed by Eq. (2), which is widely known as 'passive oxidation' characterized by an oxide film formation.



The parabolic rate law, i.e., the parabolic behavior of the $\Delta W_t/W_t$ ratio versus oxidation time, can be generally applied for the passive oxidation of a plane surface. However, we must consider in this study that an interfacial surface area between the oxide film and the fiber decreases with oxidation time, because the oxidation process is thought to start at the surface of the fiber and to move radially towards its axis. In this system, the oxidation rate is represented by the contracting-cylinder formula:⁸⁾

$$(1-X)\ln(1-X) + X = k \cdot t \quad (3)$$

where X , k , and t are an oxidation ratio of the fiber, a rate constant and oxidation time, respectively. The stoichiometry of the oxidation reaction as described in Eq. (2) provides the oxidation ratio of the fiber:

$$X = \Delta W_t / [W_o \cdot \{ (M_{\text{SiO}_2} + 0.02M_{\text{TiO}_2}) - M_{\text{STC(6)}} \} / M_{\text{STC(6)}}] \quad (4)$$

where M is molecular weight of each component is expressed as subscripts. The results shown in Fig. 1 were plotted again in Fig. 2 after applying to Eqs. (3) and (4). The kinetic data are represented fairly well by a group of straight lines at temperatures up to 1673 K, which confirms a characteristic of a diffusion-controlled mechanism. However, the plot is bent downward with the passage of about 20 ks at 1773 K, the reasons of which will be discussed in detail below.

3.2 Structure and surface morphology of oxidized fiber

Figure 3 shows the X-ray diffraction patterns of the thermal-desized STC(6) and STC(6) oxidized at

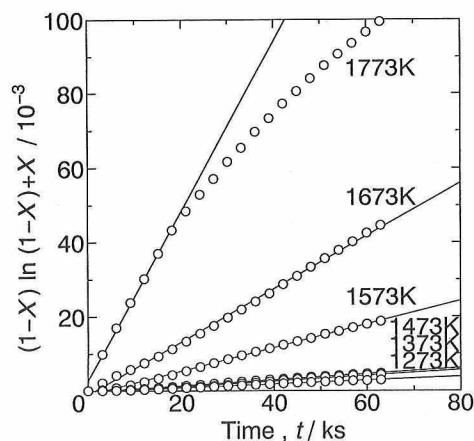


Fig. 2. Normalized plots of mass gain versus oxidation time for STC(6) from the contracting-cylinder formula (Eq. (4)).

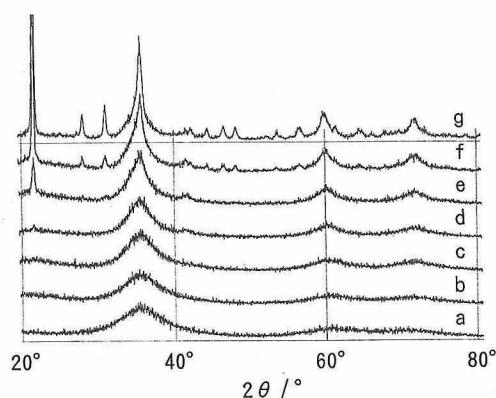


Fig. 3. XRD spectra of (a) the thermal-desized STC(6) and after oxidized ones at various temperatures (b: 1273 K, c: 1373 K, d: 1473 K, e: 1573 K, f: 1673 K and g: 1773 K).

1273, 1373, 1473, 1573, 1673 and 1773 K. The diffraction pattern of the thermal-desized fiber is broad, indicating that it is amorphous with a random atomic configuration. The fibers oxidized at 1273 and 1373 K faintly have a broad patterns at a diffraction angle of around 22° , which corresponds to the pattern of amorphous silica. In addition to amorphous silica, cristobalite is observed in the diffraction patterns of the fibers oxidized at temperatures above 1573 K. The peaks of cristobalite become sharper with the increase of heat treatment temperatures. This result almost agrees with crystal phase of a silica oxide film formed by the oxidation of SiC; silica is amorphous during the low-temperature oxidation process, and tending to be crystallized into cristobalite at higher temperatures.¹⁰⁾ The oxide film contains a small amount of TiO_2 (rutile). The most peaks of rutile overlap with cristobalite; but the presence of its have proved.⁸⁾

Figure 4 shows the SEM photographs of STC(6) after heat treatment at 1773 K. The surface of the oxide film is rough and contains many microcracks. It is necessary for a detailed discussion about the oxi-

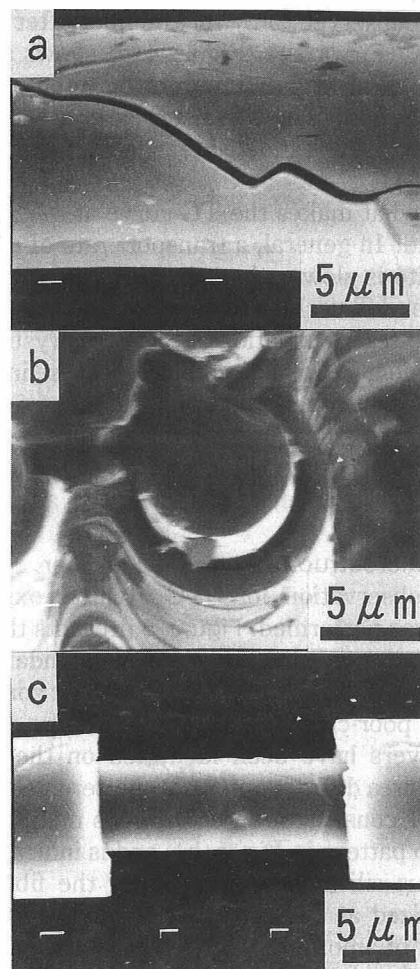


Fig. 4. SEM photographs of STC(6) after oxidized at 1773 K.

dation rate of the fiber to make clear that these microcracks were generated whether during oxidation or rapid cooling after the oxidation experiment. If the microcracks were produced during the oxidation period, they would played an important role in speeding up the diffusion rate of oxygen towards the fiber surface; that is, oxidation must have been pronounced locally near the crack ends in the oxide film.¹¹⁾ These features are not observed in Figs. 2 and 4(a); on the contrary, the decrease in the rate constant (k) with oxidation time at 1773 K is noted. It can therefore be presumed that the microcracks were not generated during the oxidation period. It is well-known that cristobalite undergoes a martensitic phase change from β - to α -cristobalite with an associated volume decrease of 5.7% at 570 K during rapidly cooling from the oxidation temperature to room temperature.¹²⁾ Tensile stress must have been generated across the film-fiber interface due to the film shrinkage. This led to produce the microcracks in the oxide film (Fig. 4(a)) and the spacings at the film-fiber interface (Fig. 4(b)). The number of defects caused by this phenomenon was proportional to the oxidation temperature: to thickness of the oxide film. Film debondings away from the fiber

were also observed, only for the fiber after oxidized at 1773 K (Fig. 4(c)). Figure 4(c) shows a feature of the crack propagation on not only the oxide film but also the core fiber; these surface cracks on the unoxidized core fiber affected tensile strength of it (see Section 3.4).

Then, what makes the TG curve at 1773 K curve downward? In general, a transport rate of oxygen in cristobalite is slower than that in amorphous silica. Costello and Tressler¹⁰ have correlated a slowing of reaction rates in oxidation of SiC with crystallization of the oxide film. In addition, the decrease in k is considered to have been due to a reduction of diffusion area resulting from the fibers sticking to each other *via* the oxide film. A number of the fibers sticking were observed especially at 1773 K, as shown in Fig. 4(b).

3.3 Microstructure of oxidized fiber

TEM observation for STC(6) after oxidized at 1773 K was performed. Figure 5 presents the photographs at the oxidized/unoxidized boundary of the fiber. Two different zones, referred to as zones 1 and 2, with a poor-characterized interface are apparent. These layers have been identified on the basis of selective-area diffraction (SAD) patterns. The external zone 1 consists of an amorphous material showing a halo pattern in Fig. 5(b), and is indicated to be amorphous silica. XRD pattern of the fiber which was oxidized at 1773 K proved that the oxide film consisted of amorphous silica, cristobalite and rutile (Fig. 3). Crystalline phases (cristobalite and rutile) in the oxide film were observed at outermost part of the fiber; however, they were cracked and debonded apart from the amorphous silica, and are not shown in Fig. 3. This debonding is supposed to have happened because of the poor adhesion between the crystalline phase and amorphous silica during the sample preparation for TEM. The fiber which was oxidized at 1773 K, therefore, exhibited three distinct parts: the crystalline phase, amorphous silica (zone 1) and the unoxidized fiber (zone 2), in order of layer from

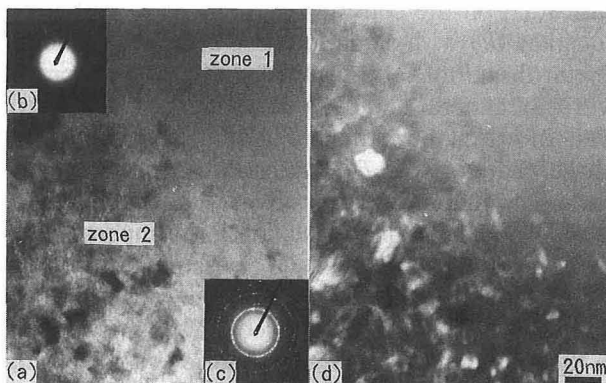


Fig. 5. TEM photographs at the oxidized/unoxidized boundary of STC(6) after oxidized at 1773 K, showing (a) BF image, (b) SAD pattern of the external zone 1, (c) that of the internal zone 2 and (d) SiC₁₁₁ DF image.

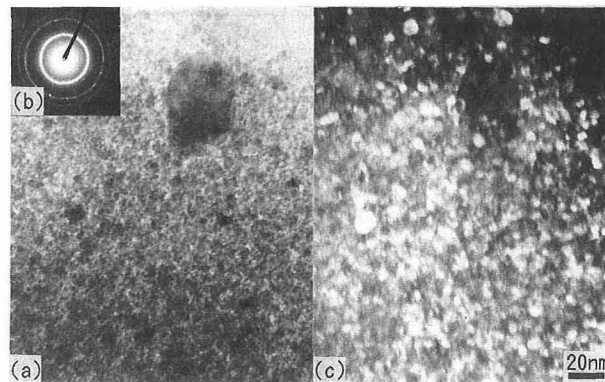


Fig. 6. TEM photographs at the unoxidized core region of STC(6) after oxidized at 1773 K, showing (a) BF image, (b) SAD pattern and (c) SiC₁₁₁ DF image.

the surface. This allows us to consider that crystallization of the oxide film begins at the O₂ gas/film surface and spreads to the film/unoxidized fiber interface.

The unoxidized zone 2 is identified as β -SiC from its SAD pattern, as shown in Fig. 5(c). Dark-field image (Fig. 5(d)), whose aperture position is in the (111) reflection ring of β -SiC, shows bright spots having the average crystallite size of 17 nm. Figure 6 presents the TEM photographs of an unoxidized core region of fiber after oxidized at 1773 K. The average size of crystallized β -SiC particles in this region is 8 nm and is too fine in comparison with that in the neighborhood at the oxidized/unoxidized boundary shown in Fig. 5(d). The crystallization of STC(6) represented by Reaction (1) starts remarkably at temperatures above 1773 K in Ar stream.⁷ On the other hand, the progress of the crystallization in O₂ stream is considered to have been suppressed when the fiber was completely covered with the oxide film. This is because the gas evolution of CO and SiO from the unoxidized core fiber could not generate except in an initial stage of the oxidation process.⁹ Consequently, this phenomenon led the average size of crystallized β -SiC particles to vary depending on locations of unoxidized regions, since the crystallization process of SiC fibers starts at the surface of the filament and moves radially towards its axis with kinetics.¹³

3.4 Tensile strength of the unoxidized core fiber

Oxide film was removed and tensile strength of the unoxidized core fiber was measured. Tensile strength is known to be controlled by Griffith flaws, and tensile testing at various gauge lengths is used to provide information on Weibull distributions of the critical flaws. The consequence of the Weibull statistics is that tensile strength at a fixed gauge length is proportional to d^{-1} (d is diameter) for surface critical flaws.² This result shows that an increase in average tensile strength with decreasing fiber diameter would be predicted. In the present study, the

unoxidized core fiber had smaller diameter with increasing oxidation temperature (Fig. 4(c)); therefore, stress values were corrected by a function of d^{-1} . The assumed stress values which the fiber would have if it has the same diameter as the original state ($d=10\ \mu\text{m}$) are shown in Fig. 7. The fibers consistently retain a strength level of 3.0 GPa up to heating temperatures as high as 1373 K. TEM examination indicated that the crystallite size of β -SiC of the fibers after oxidized at 1273 and 1373 K unchanged compared to the thermal-desized fiber's: average crystallite size of 3 nm. At temperatures of 1473 to 1673 K, the core fibers lose only about 20% of their original strength. However, the core fiber after oxidized at 1773 K loses 75% of its original strength, i.e., the average strength is 0.8 GPa. The very precipitous drop in strength over this small range of temperatures points that other effects, besides the microstructural change of the core fibers, is determinable for their strength. The major reason for the steep loss of strength appears to be the production of the microcracks (Fig. 4(c)) on the surface of the core fiber which can act as failure sites. This concept is supported by a result that the deviation of the strength for the core fiber after oxidation at 1773 K is fairly larger than others. As mentioned above, the microcracks on the surface of the core fiber are considered to have been formed mainly as a result of the phase transformation of cristobalite. In the preceding paper, we reported that the ease with which the microcracks can be formed is thought to vary greatly depending on the thickness of the oxide film (the retention time in O_2 gas stream) as well as the cooling condition which generates thermal shocks.¹⁴⁾ It is thus considered that microcracks which grow in proportion to the thickness of the oxide film will result in the low strength of the core fiber after oxidation especially at 1773 K.

3.5 Influence of the oxygen content on the oxidation mechanism of the fiber

Figure 8 shows the Arrhenius plots for the rate constants k determined from a slope of each straight lines shown in Fig. 2 (STC(6)) and those for commercial fibers, STC(18) and STC(13).⁸⁾ STC(6) has $10\ \mu\text{m}$ and the others have $8.5\ \mu\text{m}$ in diameter, as shown in Table 1. Oxidation is accelerated as fiber size decreases. Shimoo et al.¹⁵⁾ has reported that the rate constant k is inversely proportional to d^2 , so that we showed corrected k in Fig. 8. The variations of $\log k$ as a function of the reciprocal temperature in STC(18) and STC(13) are linear within the whole temperature range. The apparent energies of activation, E , are 72 kJ/mol for the former and 70 kJ/mol for the latter. These values are close to 69 kJ/mol as the energy of activation proposed for oxidation of SiC-O Nicalon® (NLM-202; Nippon Carbon Co., Ltd., Japan) fibers by Filipuzzi et al.,¹⁶⁾ however, these values are fairly lower than $E=200\text{--}300\ \text{kJ/mol}$ reported for oxidation of SiC. It is accepted that oxi-

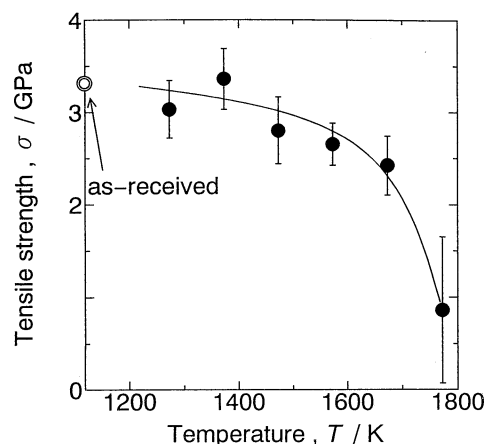


Fig. 7. Relationship between tensile strength at room temperature and the oxidation temperature. An oxide film was removed with $\text{NH}_4\text{F} + \text{HF}$ solution.

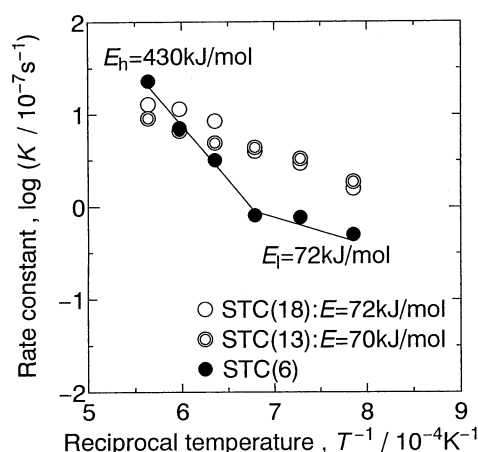


Fig. 8. Arrhenius plots for the rate constants k in Fig. 2 (STC(6)) and those in our previous data of STC(18) and STC(13) (Ref. 8).

dation of SiC is the process which is controlled by the diffusion of oxygen ions through dense oxide film.¹⁰⁾ However, the oxidation mechanism of these polymer-derived ceramic fibers presumed to be different from that of SiC. The crystal structure of the fibers is near to amorphous structure because of having large quantities of oxygen, and this results in fairly lower densities ($2.3\text{--}2.4\ \text{Mg}\cdot\text{m}^{-3}$, as shown in Table 1) of the fibers compared with that of the sintered crystalline SiC ($3.2\ \text{Mg}\cdot\text{m}^{-3}$). Therefore, it is considered that the oxide films formed on these fibers also have a large number of micropores, and that the presence of micropores leads to the low value of the apparent activation energies resulting from molecular oxygen diffusion through the oxide film. Furthermore, we consider that the micropores also result from the oxidation of free carbon present in the fiber. This point is being investigated.

Note that there are low-temperature ($T < 1473\ \text{K}$) and high-temperature ($T > 1473\ \text{K}$) regions for the

apparent energies of activation for oxidation of STC(6) alone, as shown in Fig. 8. $E_l = 72$ kJ/mol for the low-temperature region is similar to the apparent energies of activation for oxidation of STC(18) and STC(13). This supports molecular oxygen diffusion inward as a rate-controlling step at low-temperatures. On the other hand, $E_h = 430$ kJ/mol is obtained at the high-temperature region, and is much higher than E_l . The presence of these two regions has generally been reported for the activation energies of oxidation of pure SiC,¹⁷⁾ i.e., oxidation of the fiber with a low oxygen content is considered to be similar in kinetic behavior to that of pure SiC. This is correlated with the fact that the chemical composition of STC(6) is closer to SiC than that of STC(18) and STC(13), although all three fibers are fairly different in crystallinity from SiC. The rate constants k of STC(6) at low temperatures are lower than those of STC(18) and STC(13), however, tend towards values which are close together for tests performed at high temperatures. This is attributed to a mixture of network exchange diffusion and molecular oxygen diffusion.¹⁸⁾ However, it is difficult to draw conclusions about the diffusion mechanism. Further studies about this point are needed.

4. Summary

The Si-Ti-C-O fiber (STC(6)) with a low oxygen content of 6 mass% was oxidized at temperatures in the range of 1273 to 1773 K in order to measure its oxidation rate and thereby to elucidate its oxidation behavior. These results were compared to those of the commercial fibers having 18 and 13 mass%O (STC(18) and STC(13)). The kinetic data of STC(6) were expressed by the contracting-cylinder formula. The activation energies were calculated to be 72 and 430 kJ/mol at the low-temperature ($T < 1473$ K) and the high-temperature ($T > 1473$ K) regions, respectively. On the other hand, STC(18) and STC(13) had activation energies of oxidation of $E = 72$ kJ/mol and $E = 70$ kJ/mol within the whole temperature range, respectively. Oxidation of STC(6) with a low oxygen content is considered to be similar in kinetic behavior to that of pure SiC.

The oxide film consisted of SiO₂ and TiO₂; and the former was amorphous during the low-temperature oxidation process tending to be crystallized into cristobalite at higher temperatures. The average size of crystallized β -SiC particles of the interface be-

tween the oxide film and unoxidized core fiber was larger than that of core of the fiber. This is because the progress of the crystallization in O₂ stream is considered to have been suppressed when the fiber was completely covered with the oxide film. When the fiber was oxidized at 1773 K, the interface between the oxide film and the unoxidized core fiber contained many microcracks; moreover, the core fiber lost 75% of its original strength at room temperature. It is quite possible that these defects were produced by a contraction due to transformation of cristobalite (α - β) during cooling from the oxidation temperatures.

Acknowledgment This study was partly supported by a subsidy granted by the Ministry of Education, Science and Culture (No. 05650642). The authors are very grateful to Ube Industries Co., Ltd., for the supply of samples and chemical analysis, and to Dr. Seguchi (JAERI) for his help with the electron beam curing.

References

- 1) S. Yajima, K. Okamura, J. Hayashi and M. Omori, *J. Am. Ceram. Soc.*, **59**, 324-27 (1976).
- 2) J. Lipowitz, *Am. Ceram. Soc. Bull.*, **70**, 1888-94 (1991).
- 3) T. Yamamura, T. Ishikawa, M. Shibuya, T. Hisayuki and K. Okamura, *J. Mater. Sci.*, **23**, 2589-94 (1988).
- 4) L. M. Sheppard, *Am. Ceram. Soc. Bull.*, **69**, 666-73 (1990).
- 5) T. Shimoo, M. Sugimoto, Y. Kakehi and K. Okamura, *J. Japan Int. Metals*, **55**, 294-303 (1991).
- 6) K. Okamura, M. Sato, T. Seguchi and S. Kawanishi, *J. Japan Soc. Powder and Powder Metallurgy*, **35**, 170-73 (1988).
- 7) K. Kakimoto, T. Shimoo, K. Okamura, T. Seguchi, M. Sato, K. Kumagawa and T. Yamamura, *J. Japan Int. Metals*, **58**, 229-34 (1994).
- 8) T. Shimoo, Y. Kakehi, K. Kakimoto and K. Okamura, *J. Japan Int. Metals*, **56**, 175-83 (1992).
- 9) K. Kakimoto, T. Shimoo and K. Okamura, *J. Japan Int. Metals*, **57**, 957-63 (1993).
- 10) J. A. Costello and R. E. Tressler, *J. Am. Ceram. Soc.*, **69**, 674-81 (1986).
- 11) D. Mocaer, G. Chollon, R. Pailler, L. Filipuzzi and R. Naslain, *J. Mater. Sci.*, **28**, 3059-68 (1993).
- 12) C. W. Lawrence, G. A. D. Briggs, C. B. Scruby and J. R. R. Davies, *J. Mater. Sci.*, **28**, 3635-44 (1993).
- 13) J. F. Villeneuve, D. Mocaer, R. Pailler and R. Naslain, *J. Mater. Sci.*, **28**, 1227-36 (1993).
- 14) K. Kakimoto, T. Shimoo and K. Okamura, *J. Ceram. Soc. Japan*, **102**, 482-87 (1994).
- 15) T. Shimoo, H. Chen and K. Okamura, *J. Ceram. Soc. Japan*, **100**, 929-35 (1992).
- 16) L. Filipuzzi and R. Naslain, *Proceeding of 7th CIMTEC World Ceramic Congress and Satellite Symposium*, 1990, Montecatini, Italy (1990) pp. 24-30.
- 17) N. S. Jacobson, *J. Am. Ceram. Soc.*, **76**, 3-28 (1993).
- 18) Z. Zheng, R. E. Tressler and K. E. Spear, *J. Electrochem. Soc.*, **137**, 2812-16 (1990).